Journal of Materials Chemistry C

Accepted Manuscript

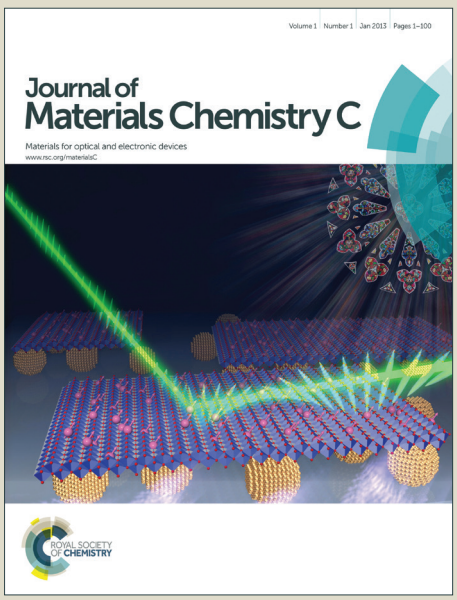

ROYAL SOCIETY OF CHEMISTRY

www.rsc.org/materialsC

Journal of Materials Chemistry C

Dynamic Article Links ►

Cite this: DOI: 10.1039/c0xx00000x

PAPER

www.rsc.org/xxxxxx

Lanthanide CPs: the Guest-Tunable Drastic Changes of Luminescent Quantum Yields, and Two Photon Luminescence

Cheng-Hui Zeng,[a, b] Jing-Ling Wang,[a] Yang-Yi Yang,*[a] Tian-Shu Chu,[a] Sheng-Liang Zhong,[b] Seik Weng Ng,[c] Wing-Tak Wong[d]

Received (in XXX, XXX) Xth XXXXXXXXX 20XX, Accepted Xth XXXXXXXXX 20XX

DOI: 10.1039/b000000x

Four kinds of guest-driven lanthanide coordination polymers (CPs) have been synthesized. They have the similar formula of $[Tb(NPA)_3CH_3CN]_n$ (**1**, H-NPA = N-phenylanthranilic acid), $\{[Tb(NPA)_3CH_3OH]CH_3OH\}_n$ (**2**), $[Ln(NPA)_3DMF]_n$ (Ln = Tb(**3a**), Gd(**3b**), Eu(**3c**)) $[Tb(NPA)_3DMSO]_n$ (**4**). These complexes were characterized by single-crystal diffraction, PXRD, FT-IR, TGA, DTA, EA, UV-vis spectra and luminescence lifetime. They are all high thermostable, acid and base resistant. The luminescence quantum yields (QY) of Tb^{3+} cpmplexes: **1**, **2**, **3a** and **4** are 4.0%, 9.0%, 44% and 46% respectively. Interestingly, there is a drastic change from 4.0% to 46% in luminescence QY by exchanging the coordination solvent, the oscillation of small molecule nearby the Tb^{3+} causes the drastic change. Furthermore, the octupolar-like structure of **4** has been found a high two-photon luminescence.

1 Introduction

The development in the field of lanthanide CPs is very rapid in the past decade because these materials possess a variety of potential applications, such as catalysis, drug delivery, supramolecular chirality, photophysics, magnetism, ion sensing and imaging.[1-14] These applications are due to the best properties of organic and inorganic components, and decrease/eliminate their drawbacks by a synergic effect. In order to get functional lanthanide materials, appropriate synthetic methods are critical. Deacon et al. contributed much to DMF and DMSO induced structural variations in rare earth benzoate complexes.[15, 16] Cepeda has studied the condition to preventing oxalate formation to participate in the structure of lanthanide CPs.[17] Gustafsson has reported single-crystal to single-crystal transformation of lanthanide CPs.[18] Paryzek has reported a solvent-controlled supramolecular self-assembly of ytterbium complex.[19] Recently Shen has reported polar solvent-water mixtures induced morphology control of lanthanide CPs,[20] some other methods of synthesizing lanthanide materials have also been reported,[21-24] but only a few works reported the solvent-tuned synthesis of lanthanide CPs.[18-21, 25-27]

[a] MOE Key Laboratory of Bioinorganic and Synthetic Chemistry, School of Chemistry and Chemical Engineering, Sun Yat-Sen University, Guangzhou, 510275, P. R. China; E-mail: cesyyy@mail.sysu.edu.cn

[b] College of chemistry and chemical engineering, Jiangxi Normal University, Nanchang, 330022, P. R. China.

[c] Department of Chemistry, University of Malaya, 50603 Kuala Lumpur, Malaysia;

[d] Department of Applied Biology and Chemical Technology, the Hong Kong Polytechnic University, P. R. China

Supporting information for this article is available on the WWW under http://www.chemeurj.org/ or from the author.

There are numerous studies of solvents effect on the luminescence properties of lanthanide complexes oligomer, however, due to the difficulties in getting accurate structural information, the effects of solvents on the lanthanide CPs luminescence has been less reported,[22, 25] with most available reports basing only on structural speculation.[28, 29] In order to get more luminescent lanthanide CPs materials, studies of solvents effect on tuning the structure of CPs, and relationship between structures and luminescence properties are imperative.

Luminescence QY is one of the important parameters for luminescent lanthanide complexes. There are three problems to be solved in preparing highly QY lanthanide complexes. First, f-f transitions in lanthanide ions are parity forbidden, the absorption coefficient is usually very low, therefore suitable antenna (usually aromatic ligands or diketon) are introduced to bind lanthanide ions, absorbing energy and transferring it to the lanthanide ions.[30] Second, the triplet excited states of the antenna should be in a suitable energy level to matches well with the emitting energy state of Ln^{3+}, but it is unlikely that the same antenna can matches well with different Ln^{3+}. Third, the energy on lanthanide ions could be easily de-excited when there are O-H, N-H or C-H groups within a radius of 20 Å.[31, 32] Robertson has been able to overcome these problems and reported some europium complexes with very high luminescence QY of 80%,[33] Raymond also reported new terbium complexes with high luminescence QY of 47.2% and 48% in 2012.[34] Some other efforts were also devoted to improve the luminescence QY of lanthanide complexes.[35-42]

Inspired by the above considerations, and our previous experience that triplet excited states of ligands with one benzene chromophore matches well with $^5D_4$ emission state of Tb^{3+},[43-45] also based on nascent studies of luminescent lanthanide complexes (non-single-crystal structure, based on structural speculation) with ligand of N-phenylanthranilic acid (H-NPA) reported by Yan and Fu.[28, 29] For further studying the relation between luminescence properties and solvent tuned structures, H-NPA was selected to synthesize single-crystal structure of Tb^{3+} complexes. Solvent effects on modifying structures and luminescence properties were investigated. These complexes were characterized by single-crystal diffraction, powder X-ray diffraction (PXRD), Fourier transform infrared (FT-IR), thermogravimetric analysis (TGA), differential thermal analysis (DTA), elemental analysis (EA), UV-visible spectra (UV-Vis) and luminescence lifetimes. Luminescence properties of the four series of Tb^{3+} CPs were systematically studied. Low luminescence QY of 4% and 9% were found in CH_3CN and CH_3OH coordination CPs **1** and **2**, respectively. But when DMF and DMSO coordinated to Tb^{3+}, the luminescence QY increased sharply to 44% and 46%, respectively. By analyzing the relationship between their structures and luminescence QY in detail, it was found that several reasons may cause the drastic changes in luminescence QY of **1**, **2**, **3a** and **4**. Besides, two photon luminescence of octupolar-like structure of **4** was also studied in detail.

2 Experimental

2.1 Materials and methods

$Tb(NO_3)_3{\cdot}6H_2O$ was prepared by dissolving Tb_4O_7 (99.9%) with concentrated HNO_3 (68%), and then evaporated at 100 ℃ until a crystal film was formed. H-NPA (99%) was purchased from Sigma-Aldrich. All other chemicals were commercially available and used without further purification.

Single crystal X-ray diffraction data were collected on a Bruker SMART 1000 CCD or Agilent 2011 diffractometer, with Cu-Kα or Mo-Kα radiation. Structures were refined by full-matrix least-squares methods with SHELXL-97 module.[46, 47] Phase purity of bulk sample was determined using a DMAX2200VPC diffractometer at 30 kV, 30 mA. TGA and DTA were performed under nitrogen atmosphere, on a Netzsch-Bruker TG-209 unit with heating rate of 10 ℃ $\cdot min^{-1}$. FT-IR was obtained in KBr pellets and recorded on a Nicolet 330 FT-IR spectrometer in the range of 4000-400 cm^{-1}. Luminescence spectra were recorded on a RF-5310PC (Shimadzu) Spectrofluorophotometer, and the excitation and emission slits were 3/3 nm. Luminescence lifetimes were collected by a combined fluorescence lifetime and steady-state spectrometer (FLSP920, Edinburgh) with a 450 W Xe lamp. The luminescence QY was determined by the

same spectrometer using a 450 W Xe lamp and an integrating sphere as our previous method.[43] Two-photon luminescence experiment was carried out as described in our previous work.[45]

2.2 Synthesis of $[Tb(NPA)_3CH_3CN]_n$ (1)

H-NPA (39.6 mg, 0.24 mmol) and 15 ml water were mixed and the pH value was adjusted to about 9 with 0.1 M NaOH solution. 25 ml CH_3CN including 4.5 mg $Tb(NO_3)_3·6H_2O$ (0.01 mmol) was slowly added to the ligand solution, making the system into two layers, and sealed in a long test tube and keeping still for 3 weeks at room temperature about 21-32 ℃, yellow needle-like crystals were obtained. Yield: 50.1% based on Tb^{3+}. Anal. Calcd (%): C, 58.86; H, 3.975. Found (%): C, 58.57; H, 3.941. FT-IR (Figure S1b) (KBr pellet, cm^{-1}): 3323 (s), 1595 (m), 1576 (m), 1541 (m), 1502 (s), 1398 (s), 1282 (s), 1159 (m), 1045 (m), 893 (w), 810 (w), 750 (s), 1168 (m), 696 (m), 553 (w), 523 (w).

2.3 Synthesis of $\{[Tb(NPA)_3CH_3OH]CH_3OH\}_n$ (2)

$Tb(NO_3)_3·6H_2O$ (0.03 mmol) and H-NPA (0.09 mmol) were mixed in a 24 ml solution of H_2O/CH_3OH (V : V = 1 : 3). 0.1 M NaOH aqueous solution was added dropwise and the pH value was adjusted to 6.5. The resulting mixture was sealed into a Teflon reactor and heated at 80 ℃ for 3 days under autogenous pressure, then cooled to room temperature naturally followed by slow evaporation for three weeks. Yellow prism crystals of **2** were then obtained. Yield: 19.3% based on Tb^{3+}. Anal. Calcd (%): C, 57.28; H, 4.455. Found (%): C, 57.32; H, 4.501. FT-IR (Figure S1a) (KBr pellet, cm^{-1}): 3432 (s), 2920 (m), 1498 (s), 1406 (s), 1279 (s), 1157 (m), 1115 (m), 1074 (m), 1030 (w), 893 (w), 748 (m), 675 (w).

2.4 Synthesis of $[Ln(NPA)_3DMF]_n$ (Ln = Tb(3a), Gd(3b), Eu(3c))

The synthesis procedure for **3a**, **3b** and **3c** were similar. 0.03 mmol Ln $(NO_3)_3·6H_2O$ and 0.09 mmol H-NPA were mixed in 24 ml solution of H_2O/DMF (V : V = 1 : 3). Then 0.1 M NaOH solution was added dropwise to adjust the pH to about 6.5. The mixture was sealed into a 10 ml Teflon reactor and heated at 80℃ for 3 days, then cooled to room temperature naturally. Colorless block crystals were obtained.

$[Tb(NPA)_3·DMF]_n$ (3a) Yield: 33.7% based on Tb^{3+}. Anal. Calcd (%): C, 58.07; H, 4.293. Found (%): C, 58.17; H, 4.271. FT-IR (Figure S1d) (KBr pellet, cm^{-1}): 3305 (s), 3039 (m), 2931 (w), 1936 (w), 1670 (m), 1612 (s), 1597 (s), 1543 (m), 1502 (s), 1448 (m), 1396 (s), 1282 (s), 1161 (w), 750 (m), 696 (m), 523 (w).

$[Gd(NPA)_3·DMF]_n$ (3b) Yield: 32.1% based on Tb^{3+}. Anal. Calcd (%): C, 58.18; H, 4.301. Found (%): C, 58.17; H, 4.311. FT-IR (Figure S1e) (KBr pellet, cm^{-1}): 3305 (s), 3041 (m), 2931 (w), 1936 (w), 1670 (m), 1612 (s), 1597 (s), 1543 (m), 1500 (s), 1446 (m), 1396 (s), 1282 (s), 1161 (w), 748 (m), 696 (m), 523 (w).

$[Eu(NPA)_3·DMF]_n$ (3c) Yield: 27.3% based on Tb^{3+}. Anal. Calcd (%): C, 58.54; H, 4.327. Found (%): C, 58.59; H, 4.332. FT-IR (Figure S1f) (KBr pellet, cm-1): 3303 (s), 3041 (m), 2931 (w), 1936 (w), 1670 (m), 1612 (s), 1597 (s), 1541 (m), 1500 (s), 1448 (m), 1396 (s), 1282 (s), 1161 (w), 748 (m), 696 (m), 523 (w).

2.5 Synthesis of $[Tb(NPA)_3DMSO]_n$ (4)

$Tb(NO_3)_3·6H_2O$ (0.03 mmol) and H-NPA (0.09 mmol) were mixed in 18 ml solution of H_2O/DMSO (V : V = 1 : 1). 0.1 M NaOH aqueous solution was added and the pH value was adjusted to 6.5. The mixture was sealed into Teflon reactor and heated at 80 ℃ for 3 days, then cooled to room temperature slowly. Colorless block crystals were obtained. Yield: 31.3% based on Tb^{3+}. Anal. Calcd (%): C, 56.36; H, 4.153. Found (%): C, 56.32; H, 4.131. FT-IR (Figure S1c) (KBr pellet, cm^{-1}): 3398 (s), 3034 (m), 2916 (w), 1936 (w), 1595 (s), 1541 (s), 1502 (s), 1448 (m), 1398 (s), 1282 (s), 1161 (w), 1011 (m), 958 (w), 752 (m), 698 (m), 523 (w).

3 Results and discussion

3.1 Syntheses

When H-NPA and $Tb(NO_3)_3·6H_2O$ were mixed in two layer solutions of H_2O and CH_3CN, respectively, we got single crystal **1**. X-ray diffraction data and elemental analysis results revealed that one CH_3CN coordinated to Tb^{3+}, the coordinated CH_3CN is

among the big ligands of NPA and may play the role of satisfying high coordination number of Tb^{3+}. This encouraged us to synthesize more single crystals by replacing CH_3CN with small molecules such as CH_3OH, C_2H_5OH, DMF, DMSO, H_2O, pyridine, acetone or acetylacetone. After ten months of efforts, small molecules of CH_3OH, DMF and DMSO were assembled to Tb^{3+} in crystals **2**, **3a** and **4** (Figure 1) by different synthetic procedures. In synthesizing **1**, the pH of ligand solution was 9, which was different from the pH = 6.5 of ligand solutions in synthesizing **2**, **3a**, **3b**, **3c** and **4,** so the pH value may also have effects on the crystal structures. Since these structures are very similar, **1** and **2** even have the same space group of C2/c, single-crystal-to-single-crystal (SCSC) transform experiments were performed. When **1** was immersed in CH_3OH, DMSO or DMF; **2** was soaked in CH_3CN, DMSO or DMF, **3a** was soaked in CH_3OH, CH_3CN or DMSO, **4** was soaked in CH_3OH, CH_3CN or DMF for three weeks, single crystal data and PXRD experiment results (not shown) indicated that the crystal structures did not change, inferred that SCSC did not happen. These might due to the steric hindrance of phenylamino that prevented the coordinated solvent escaping and prevented the vast peripheral solvent getting into the cavities encompassed by ligands, and also infer the excellent stability of these complexes.

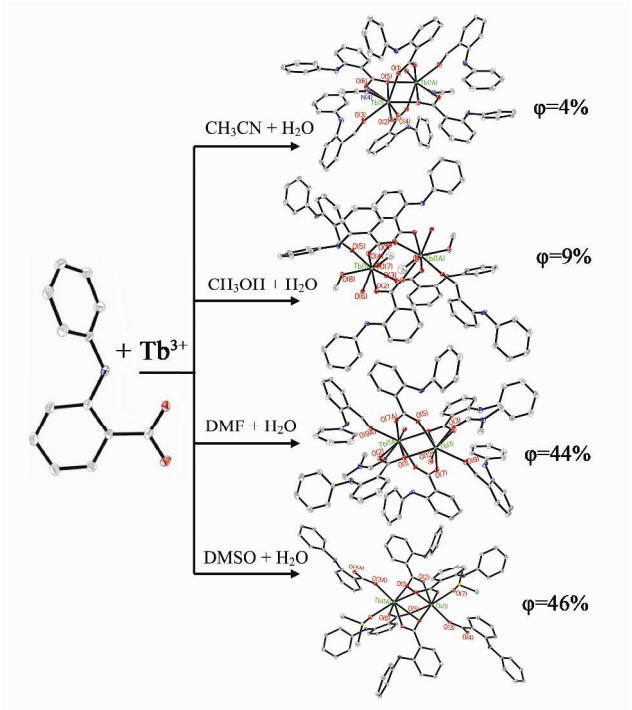

Figure 1. Guest-driven approach to synthesize four kinds of lanthanide CPs and comparison of their luminescence QY.

Table 1. Crystallographic data of **1**, **2**, **3a**, **3b**, **3c** and **4**.

Complex	1	2	3a	3b	3c	4
Empirical formula	$TbC_{41}H_{33}N_4O_6$	$TbC_{41}H_{38}N_3O_8$	$TbC_{42}H_{37}N_4O_7$	$GdC_{42}H_{37}N_4O_7$	$EuC_{42}H_{37}N_4O_7$	$TbC_{41}H_{36}N_3O_7S$
Formula weight	836.63	859.66	868.69	867.01	861.72	873.71
Temperature / K	293(2)	173(2)	293(2)	100(2)	100(2)	100(2)
Wavelength / Å	1.54178	0.71073	1.54178	1.54184	1.54184	1.54184
Crystal system	Monoclinic	Monoclinic	Triclinic	Triclinic	Triclinic	Monoclinic
Space group	C2/c	C2/c	P-1	P-1	P-1	P21/c
a / Å	37.5637(19)	37.712(6)	9.2946(7)	9.2990(2)	9.2927(3)	13.8541(3)
b / Å	9.1926(2)	9.3734(14)	13.8614(9)	13.8249(4)	13.8088(3)	28.4336(6)
c / Å	26.6219(14)	26.150(4)	14.4942(8)	14.4792(4)	14.4762(5)	9.3044(2)
α / (°)	90	90	97.275(5)	97.345(2)	97.319(2)	90
β / (°)	129.649(8)	129.367(2)	96.048(5)	96.112(2)	96.124(3)	97.754(2)
γ / (°)	90	90	98.684(6)	98.502(2)	98.362(2)	90
V / Å3	7078.1(9)	7146.4(18)	1816.3(2)	1810.88(8)	1807.98(9)	3631.69(13)
Z	8	8	2	2	2	4
Calculated density/mg·m^{-3}	1.570	1.598	1.588	1.590	1.583	1.598
F(000)	3360	3472	876	874	872	1760
Crystal size/mm	0.30×0.10×0.10	0.18×0.13×0.07	0.13×0.12×0.11	0.20×0.10×0.05	0.20×0.10×0.05	0.40×0.04×0.04
Theta range for data collection / (°)	3.06 to 62.46	2.01 to 25.01	3.10 to 62.61	3.10 to 76.78	3.10 to 76.93	3.11 to 76.72
Reflections collected / unique	11744/5548 [R(int) = 0.0373]	15046/6189 [R(int) = 0.0272]	9171/5630 [R(int) = 0.0625]	36689/7584 [R(int) = 0.1298]	24854/7580 [R(int) = 0.0370]	20851/7577 [R(int) = 0.0491]
Data / restraints /	5548/1/470	6189/4/486	5630/0/487	7584/318/489	13031/318/485	7577/306/478

parameters						
Goodness-of-fit on F^2	1.046	0.967	1.048	1.109	1.142	1.295
Final R indices [I > 2sigma(I)][a]	R1 = 0.0287, wR2 = 0.0747	R1 = 0.0285, wR2 = 0.0746	R1 = 0.0424, wR2 = 0.1085	R1 = 0.0618, wR2 = 0.1721	R1 = 0.0809, wR2 = 0.2382	R1 = 0.0891, wR2 = 0.2204
R indices (all data)	R1 = 0.0307, wR2 = 0.0765	R1 = 0.0428, wR2 = 0.0837	R1 = 0.0449, wR2 = 0.1108	R1 = 0.0649, wR2 = 0.1742	R1 = 0.0846, wR2 = 0.2421	R1 = 0.0948, wR2 = 0.2227

[a] $R = \sum||Fo| - |Fc||/\sum|Fo|$, $wR = [\sum w(|Fo^2| - |Fc^2|)^2/\sum w(|Fo^2|)^2]^{1/2}$

3.2 Structural analysis

Crystallographic data and structural refinement parameters for **1**, **2**, **3a**, **3b**, **3c** and **4** are listed in Table 1. Selective bond lengths and angles for these complexes are listed in table S1 (ESI†).

Complex **1** has the space group of C2/c (No. 15), it is constructed by dinuclear SBUs and featured a 1D structure of $[Tb(NPA)_3CH_3CN]_n$ in the *ob* direction. Each second building units (SBU) consists two equivalent Tb^{3+}, six NPA, two coordination CH_3CN (Figure 2-I), the packing is shown in Figure 2-II and the 1D structure is similar to a butterfly (Figure 3). Tb^{3+} is eight coordinated by one N from CH_3CN and seven O of carboxyl, the eight coordinated atoms are arranged in the mode of distorted dicapped prism (Figure S2). Bond lengths of Tb-O are among 2.226-2.877 Å, the longer Tb···Tb distance of 5.386 Å is bridged by two carboxyl, and the shorter distance of Tb···Tb is 3.98 Å, which is bridged by four carboxyl, two O bridged mode make the Tb···Tb distance even shorter than **1** which bridged by four carboxyls (Figure 4). This is consistent with our previous result that stronger bridge forth would pull the metal ions closer.[45] Ligands in **1** have two kinds coordination mode of μ_2-η^2-η^1 and μ_2-η^1-η^1 (Figure S3). Experimental PXRD pattern corresponded well with the results simulated from single-crystal **1**, indicating high phase purity of powder sample (Figure S4). When **1** was immersed in pH = 1 and pH = 12 water solutions for one week, the main peaks of PXRD patterns matched well with the simulated results of **1**. This confirmed **1** is an acid- and alkali-resistant material.

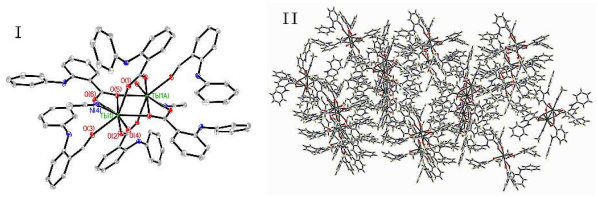

Figure 2. I) ORTEP view (30% thermal ellipsoids) shows the coordination environment and SBU of **1**. All the hydrogen atoms are omitted, only Tb and coordinating atoms are labeled for clarity; II) Packing diagram of **1**.

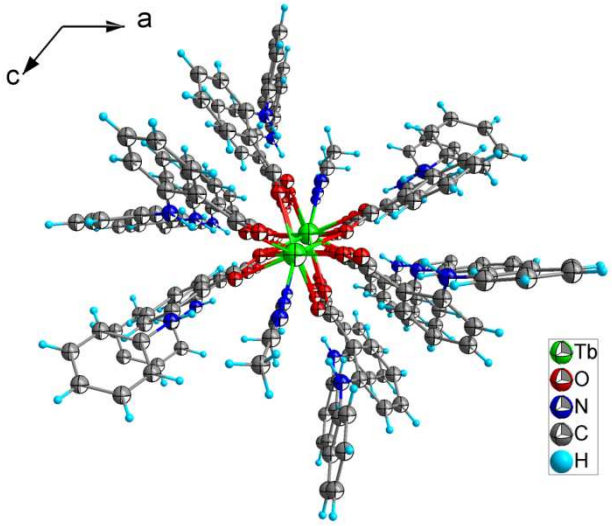

Figure 3. Octupolar-like structure of **1** along the *ob* direction.

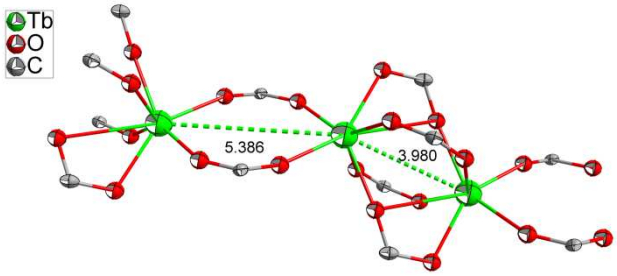

Figure 4. Short and long Tb···Tb distances in **1**.

Complex **2** featured a 1D structure of $\{[Tb(NPA)_3CH_3OH]CH_3OH\}_n$. It has the same space group as **1**, the cell parameters of **1** and **2** are very similar (Table 1, cell volume difference is as small as 0.45%), we think the very small difference is induced by instrumental error or calculation error, but not induced by the coordination solvents. **2** is constructed by dinuclear SBUs (Figure 5-I), each SBU consists two equivalent Tb^{3+}, six deprotonated ligands NPA, two coordination CH_3OH and two crystalline CH_3OH molecules. SBU is connected by ligands to form a 1D chain in the *ob* direction; SBUs stretch to form the packing structure of Figure 5-II. 1D chain of **2** looks

like a spider from the *ob* direction (Figure S5). Tb^{3+} is coordinated by seven O, not in the range of most coordination number of 8-9. The seven O around Tb^{3+} are arranged in a distorted one-capped triangular prism (Figure S6a). Ligands in **2** have only one coordination mode of μ_2-η^1-η^1 to bridge two Tb^{3+} (Figure S6b). Bond lengths of Tb-O are among 2.269-2.486 Å, which are usually seen in other lanthanide complexes. [48, 49] Distances of Tb···Tb are 4.216 and 5.294 Å, the shorter distance of 4.216 Å is bridged by stronger strength of four carboxylic acid, and the longer distance of 5.294 is bridged by only two carboxyls (Figure S7). PXRD patterns corresponded well with the results simulated from the single-crystal **2**, indicating the high phase purity of bulk sample (Figure S8).

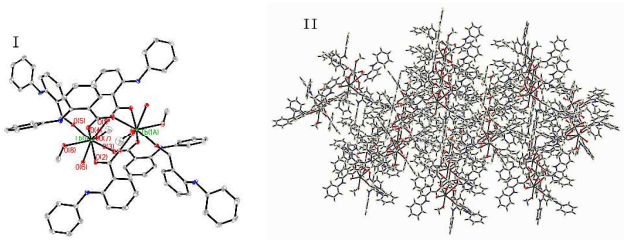

Figure 5. I) ORTEP view (30% thermal ellipsoids) shows the coordination environment and SBU of **2**. All the hydrogen atoms are omitted, only Tb and coordinated atoms are labeled for clarity; II) Packing diagram of **2**.

Single crystal data (table 1) reveals that complexes **3a**, **3b** and **3c** are isostructural and all featured a 1D structure of $[Ln(NPA)_3DMSO]_n$ (Ln = Tb(**3a**), Gd(**3b**), Eu(**3c**)). As an example, structure **3a** would be described in detail.

3a belongs to the triclinic space group P-1 (No. 2), SBUs (Figure 6-I) extend to form a packing structure of Figure 6-II. 1D structure of **3a** extends in *oa* direction (Figure S9).[50, 51] Eight O around Tb^{3+} are arranged in a distorted bi-capped triangular prism (Figure S10). The Tb···Tb distances are 5.535 and 4.028, similar to **1**, longer Tb···Tb distance is bridged by two carboxyl, shorter Tb···Tb distance is bridged by four carboxyl and two O (Figure S11). PXRD experiment indicating a high phase purity of the powder samples **3a** (Figure S12). The acid and base resistance experiment was done with the same procedure as **1**; results showed that **3a** is an excellent acid- and alkali-resistant material.

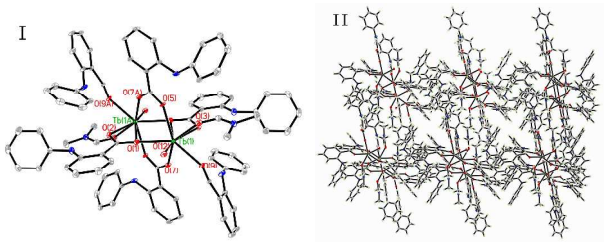

Figure 6. I) ORTEP view (30% thermal ellipsoids) shows the coordination environment and SBU of **3a**. All hydrogen atoms are omitted; only Tb and coordination atoms are labeled for clarity; II) Packing diagram of **3a**.

Complex **4** has the formular of $[Tb(NPA)_3DMSO]_n$ and crystallizes in the monoclinic space group P21/c (No. 14). Packing structure of **4** was constructed by dinuclear SBUs (Figure 7) and featured octupolar-like 1D structure along the *ob* direction (Figure S13). Bond lengths of Tb-O were among 2.269-2.486 Å. NPA in **4** has the same coordination modes as **1**. Similar to complex **1**, the Tb···Tb distance in **4** are 5.576 and 3.979 Å (Figure S14). PXRD indicated high phase purity of powder sample **4**. When **4** was soaked in pH = 1 and pH = 12 water solutions for one week, the main peaks of PXRD matched well with the simulated results of single crystal **4** and proved that **4** is stable material in acid and base environment (Figure S15).

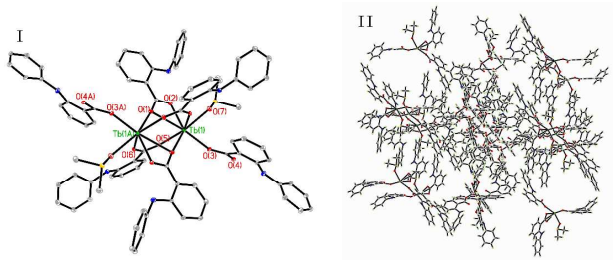

Figure 7. I) ORTEP view (30% thermal ellipsoids) shows the coordination environment and SBU of **4**. All hydrogen atoms are omitted; only Tb and coordination atoms are labeled for clarity; II) Packing diagram of **4**.

3.3 Thermogravimetric analyses

Figure 8(II) showed the TGA and DTA curves of complex **2**. The TGA plot showed a weight loss of 3.81% before 65 ℃, which corresponding to one crystalline CH_3OH loss (calculated: 3.72%). From 65 to 379 ℃, there was another weight loss of 3.78%, which corresponded to one coordination CH_3OH

(calculated: 3.72%) on each Tb^{3+}. There was another obvious weight loss from 379 ℃ to the end, which corresponded to the decomposition of ligands. Figure 15(I), (III) and (IV) showed similar TGA and DTA behaviors of sample **1**, **3a** and **4**, respectively. TGA plots show a weight loss of 4.96% before 183 ℃, 2.28% before 201 ℃ and 8.99% before 232 ℃, that corresponded to one coordinated CH_3CN, DMF and DMSO loss on each Tb^{3+} in **1**, **3a** and **4** (calculated: 4.91%, 7.03% and 8.94%), respectively. From 377, 370 and 383 ℃, the ligands in **1**, **3a** and **4** began to decompose, respectively. The DTA curve showed two big endothermic peaks during this process, which indicated the ligands in these complexes decomposed in two steps.

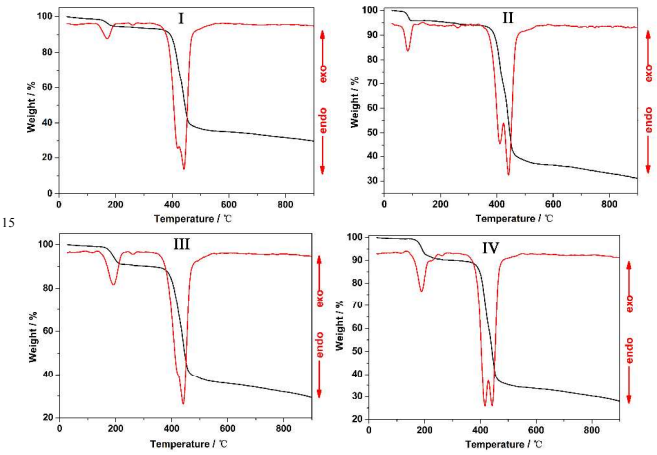

Figure 8. TGA and DTA curves of I, II, III and IV for **1**, **2**, **3a** and **4**, respectively.

3.4 UV-vis spectra analysis

UV-vis spectra of complexes **1**, **2**, **3a** and **4**, together with the ligand of H-NPA in four different solvents, are shown in Figure S16. Table 2 showed the UV-vis spectra parameters of these complexes. Coordination complexes and ligand exhibited intense absorption bands at ca. 340 nm, which could be assigned to the n–π* transition of ligand. It was obvious that the n–π* transitions of Tb^{3+} complexes were slightly bathochromically-shifted. It could be seen that the absorption intensities (A) and molar absorption coefficient values (E) of complexes **2**, **3a** and **4** were nearly three times as that of ligand, because there were three ligands coordinated to every Tb^{3+}. The A and E values of H-NPA and complex **1** are similar, which might be due to bad solubility of **1** in CH_3CN.

Table 2. UV-vis spectra parameters of **1**, **2**, **3a**, **4** and ligand.

Comp.	medium	C/mol·L^{-1}	λ/nm	A	E/ dm^2·mol^{-1}
1	CH_3CN	1×10^{-5}	349	0.310	3.10×10^5
H-NAP			347	0.304	3.04×10^5
2	CH_3OH	8×10^{-5}	341	0.593	7.41×10^4
H-NAP			338	0.201	2.51×10^4
3a	DMF	2×10^{-5}	347	0.817	4.35×10^5
H-NAP			345	0.269	1.43×10^5
4	DMSO	5×10^{-5}	343	0.636	1.27×10^5
H-NAP			340	0.221	4.42×10^2

3.5 One photon luminescence

Luminescent properties of **1**, **2**, **3a** and **4** were investigated in the solid state at room temperature. As shown in Figure 9, under the best excitations of 391, 399, 396 and 409 nm, respectively, these complexes displayed characteristic emission bands of Tb^{3+} at about 489, 545, 586 and 622 nm, which were assigned to the characteristic transitions of $^5D_4$–$^7F_6$, $^5D_4$–$^7F_5$, $^5D_4$–$^7F_4$ and $^5D_4$–$^7F_3$ of Tb^{3+}, respectively.

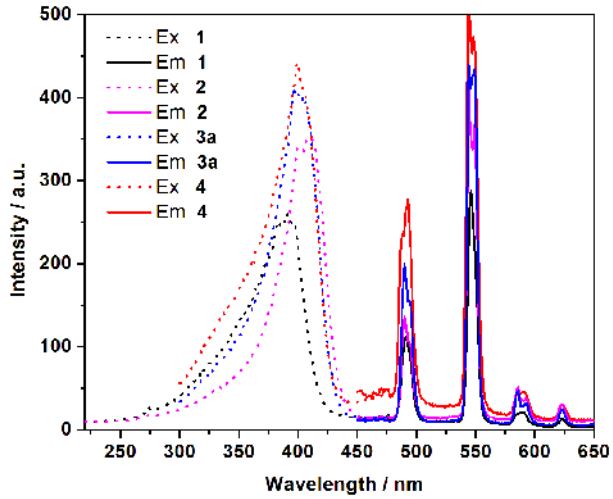

Figure 9. Excitation and emission spectra of **1**, **2**, **3a** and **4**.

The total luminescence QY of Tb^{3+}-centered complexes **1**, **2**, **3a** and **4** are 4.0%, 9.0%, 44% and 46%, under the best excitations of 399, 391, 409 and 396 nm, respectively. The overall luminescence QY of these complexes are in the order of **4** ＞**3a**＞**2**＞**1**. Luminescence QY of complexes **3a** and **4** are obviously larger than those of **1** and **2**, **3a** and **4** are ten more times than **1**, four times as that of **2**. Since the antenna of NPA and its number in these four lanthanide CPs are the same and

only coordination solvents are different, several reasons such as weight atom in coordination molecule; distance between Tb^{3+} and oscillators; oscillator number and hydrogen bond which fix the oscillator, which effect the energy lose on Tb^{3+} through oscillation of C-H, N-H and O-H groups within a radius of 20 Å were analyzed in detail.[31, 32] **4** exhibits the largest luminescence QY in the four complexes, and the luminescence QY of 46% is also a very high value in terbium complexes. Comparing with CH_3OH, CH_3CN and DMF, the heavy atom of S in coordination solvent of DMSO would decrease the oscillation of oscillator, which could decrease the energy lose on Tb^{3+} through non-radiation. **3a** also has highly luminescence QY of 44%, and this may due to the long distance between oscillators(H-C-N-C-O) and Tb^{3+}. Although **2** has more oscillators and the distances between oscillators and Tb^{3+} center are nearer than **1**, **2** has larger luminescence QY. This can be ascribed to the hydrogen bond of oscillators, in **2**, the very near oscillator of O-H is fixed by a short (2.502 Å) and tight hydrogen bond (figure S17), two of other three oscillators of C-H on methyl group are also fixed by hydrogen bond, but only one oscillator of C-H in CH_3CN is fixed by hydrogen. The high luminescence QY of complexes **4** and **3a** suggest the triplet energy state of ligand NPA matches well with the $^5D_4$ emission state of Tb^{3+}.

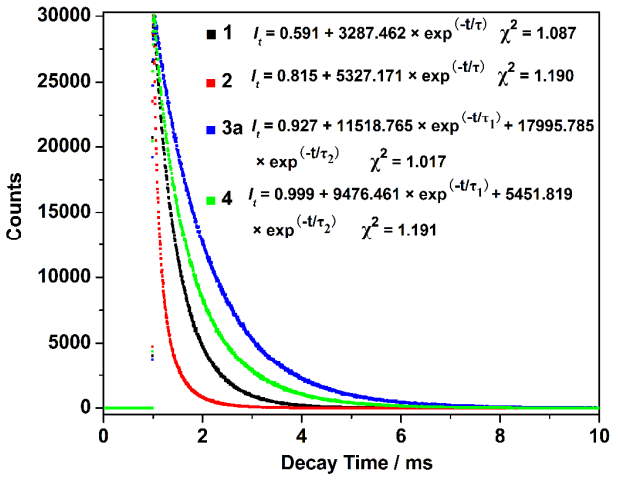

Figure 10. Luminescence lifetimes of solid samples of **1**, **2**, **3a** and **4** at room temperature.

Luminescence lifetimes of complexes **1**, **2**, **3a** and **4** were investigated in solid state. The curves of the luminescence decay at 545 nm were illustrated in Figure 10. Complexes **1** and **2** followed single exponential decay law, and the equation of $I_t = A_0 + A_1 \times \exp(-t/\tau)$ (τ is the luminescence lifetime, A_0 and A_1 are the weighting parameters) was utilized for fitting the luminescence decay curves, lifetime values were determined to be 0.419 and 0.635 ms for **1** and **2**, respectively. The decay curves for complexes **3a** and **4** could fit well to the function of $I_t = A_0 + A_1 \times \exp(-t/\tau_1) + A_2 \times \exp(-t/\tau_2)$ (τ_1 and τ_2 are the fast and slow components of the luminescence lifetimes, A_0, A_1 and A_2 are the weighting parameters), and the luminescence lifetime values for **3a** and **4** were 1.192 and 0.917 ms. Luminescence lifetimes of four complexes were in the order of **4**＞**3a**＞**2**＞**1**, which was consistent with the results of luminescence QY described above.

3.6 Two-photon luminescence

Since complexes **4** has very high QY and is similar to octupolar organic structures, which are apt to show two-photon absorption,[50, 51] the upconversion luminescence of **4** was studied. When solid sample **4** was excited by an 800 nm picosecond laser at different power densities, a strong two-photon absorption inducing luminescence could be seen (Figure 11). The characteristic emission bands of Tb^{3+} at about 489, 542, 590 and 619 nm could be detected, which were assigned to the transitions of $^5D_4$–$^7F_6$, $^5D_4$–$^7F_5$, $^5D_4$–$^7F_4$ and $^5D_4$–$^7F_3$, respectively. In this study, two-photon luminescence signal was clear when the input power decreased to 0.532 μJ, it is much stronger than our previous results in which the two-photon luminescence can nearly not be seen when the input power was 11.0 μJ at the same instrument.[45] And this infers a highly two-photon luminescence of the highly luminescence QY of **4**.

Multiple-photon luminescence intensity and pump power density can be expressed as follows:

$$I_{up} \propto I_{pump}^{n} \qquad (1)$$

Where I_{up} is the intensity of multi-photon luminescence, I_{pump} is the pump power density of laser, n is the number of photons involved in the absorption processes, which can be experimentally determined from a *log–log* plot between luminescence intensity and pump power density. Figure 15 shows the slope of the double logarithmic fitted line at 545 nm is 1.9172, which is very close to 2, indicating two-photon excitation dominated this process.[50]

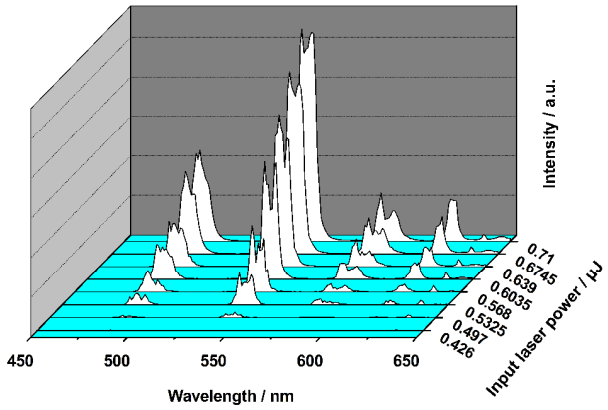

Figure 11. Luminescence intensity depends on input laser powder for **4**.

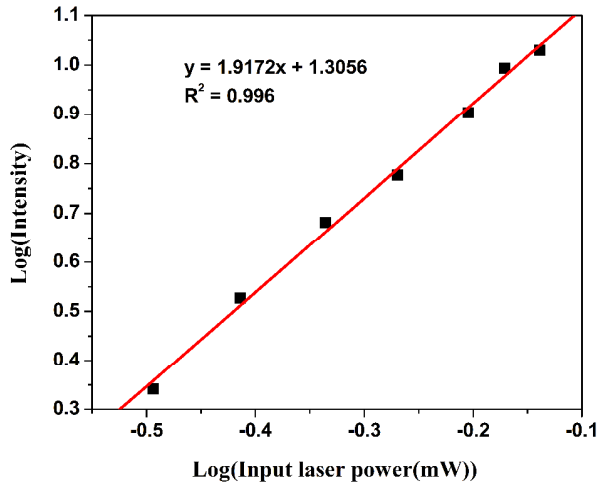

Figure 12. Two photon luminescence intensity for **4** depends on the pump power density.

One and two 800 nm photons have the energy of 12 500 and 25 000 cm^{-1}, respectively. The near energy gap of $^5D_3$–$^7F_6$ and $^5D_4$–$^7F_6$ is 26336 and 20545 cm^{-1} for Tb^{3+}. There is no energy level suitable to accept one or two photons' energy directly, hence, we think the luminescence of Tb^{3+} might be induced by two-photon absorption (TPA) of ligand.[52] When the focal lens in the optical path was removed from the excitation path or the laser power was lowered by a factor of 100, the Tb^{3+}-centred emission could be observed. These results were contrary to the direct two photon excitation of lanthanide ions reported by Sørensen.[53] It further confirmed that the two-photon luminescence mechanism was induced by TPA of the ligand. The possible two photon luminescence process/mechanism for **4** is similar to our previous result.[45]

4 Conclusions

In summary, four kinds of lanthanide CPs were synthesized with the guest-driven approach. They were characterized by single-crystal diffraction, PXRD, EA, FT-IR, UV-vis spectra and luminescence lifetime. These complexes were thermostable, acid- and base-resistant materials. The luminescence QY of **1**, **2**, **3a** and **4** are 4.0%, 9.0%, 44% and 46%, in which there is a drastic change from 4.0% to 46%. The oscillation of small molecule nearby the Tb^{3+} affects the luminescent QY, weight atom in coordination molecule, distance between Tb^{3+} and oscillators, oscillator number and hydrogen bonds which fix the oscillators could change the energy transmitting to Tb^{3+}, and lead to the QY alter dramatically. The octupolar-like structure of **4** was found a high two-photon luminescence, which will have potential application in infrared imaging for the living cell.

Acknowledgements

The authors acknowledge the financial support of National Natural Science Foundation of China (NO. 20973203, 91022012), the Fundamental Research Funds for the Central Universities, and the Ministry of Higher Education of Malaysia (grant No. UM.C/HIR/MOHE/SC/12).

Notes and references

1. S. J. Butler and D. Parker, *Chem. Soc. Rev.*, 2013, **42**, 1652-1666.
2. F. T. Edelmann, *Chem. Soc. Rev.*, 2012, **41**, 7657-7672.
3. M. Schaferling, *Angew. Chem. Int. Edit.*, 2012, **51**, 3532-3554.
4. S. V. Eliseeva and J. C. G. Bunzli, *Chem. Soc. Rev.*, 2010, **39**, 189-227.
5. J. Feng and H. J. Zhang, *Chem. Soc. Rev.*, 2013, **42**, 387-410.
6. M. Ballesteros-Rivas, H. H. Zhao, A. Prosvirin, E. W. Reinheimer, R. A. Toscano, J. Valdes-Martinez and K. R. Dunbar, *Angew. Chem. Int. Edit.*, 2012, **51**, 5124-5128.
7. Z. S. Pillai, P. Ceroni, M. Kubeil, J.-M. Heldt, H. Stephan and G. Bergamini, *Chem-Asian J*, 2013, **8**, 771-777.
8. K. Miyata, Y. Konno, T. Nakanishi, A. Kobayashi, M. Kato, K. Fushimi and Y. Hasegawa, *Angew. Chem. Int. Edit.*, 2013, **52**, 6413-6416.
9. Y. Q. Xiao, Y. J. Cui, Q. A. Zheng, S. C. Xiang, G. D. Qian and B. L. Chen, *Chem. Commun.*, 2010, **46**, 5503-5505.
10. B. Chen, S. Xiang and G. Qian, *Accounts Chem Res*, 2010, **43**, 1115-1124.
11. Y.-M. Zhu, C.-H. Zeng, T.-S. Chu, H.-M. Wang, Y.-Y. Yang, Y.-X. Tong, C.-Y. Su and W.-T. Wong, *J. Mater. Chem. A*, 2013, **1**, 11312-11319.

12. C.-F. Chow, M. H. W. Lam and W.-Y. Wong, *Anal Chem*, 2013, **85**, 8246-8253.
13. J. Yu, Y. Cui, H. Xu, Y. Yang, Z. Wang, B. Chen and G. Qian, *Nat. Commun.*, 2013, **4**.
14. Y. Cui, Y. Yue, G. Qian and B. Chen, *Chem Rev*, 2012, **112**, 1126-1162.
15. H. Busskamp, G. B. Deacon, M. Hilder, P. C. Junk, U. H. Kynast, W. W. Lee and D. R. Turner, *Crystengcomm*, 2007, **9**, 394-411.
16. G. B. Deacon, S. Hein, P. C. Junk, T. Juestel, W. Lee and D. R. Turner, *Crystengcomm*, 2007, **9**, 1110-1123.
17. J. Cepeda, R. Balda, G. Beobide, O. Castillo, J. Fernandez, A. Luque, S. Perez-Yanez and P. Roman, *Inorg. Chem.*, 2012, **51**, 7875-7888.
18. M. Gustafsson, J. Su, H. J. Yue, Q. X. Yao and X. D. Zou, *Cryst. Growth. Des.*, 2012, **12**, 3243-3249.
19. V. Patroniak, M. Kubicki, A. Mondry, J. Lisowski and W. Radecka-Paryzek, *Dalton Trans.*, 2004, 3295-3304.
20. S. Wang, B. Zhang, Y. Hou, C. Du and Y. Wu, *J. Mater. Chem. C*, 2013, **1**, 406-409.
21. S. Mishra, E. Jeanneau, H. Chermette, S. Daniele and L. G. Hubert-Pfalzgraf, *Dalton Trans.*, 2008, 620-630.
22. A. A. Ansari, N. Singh, A. F. Khan, S. P. Singh and K. Iftikhar, *J. Lumin.*, 2007, **127**, 446-452.
23. K. Miyata, T. Nakanishi, K. Fushimi and Y. Hasegawa, *J. Photoch. Photobio. A*, 2012, **235**, 35-39.
24. C. L. Pan, W. Chen and J. F. Song, *Organometallics*, 2011, **30**, 2252-2260.
25. J. R. Li, R. H. Zhang and X. H. Bu, *Aust. J. Chem.*, 2008, **61**, 115-121.
26. W. Y. Bi, X. Q. Lu, W. L. Chai, W. J. Jin, J. R. Song and W. K. Wong, *Inorg. Chem. Commun.*, 2008, **11**, 1316-1319.
27. Z. Spichal, J. Pinkas and M. Necas, *Polyhedron*, 2012, **48**, 99-103.
28. B. Yan, H. Zhang, S. Wang and J. Ni, *J. Photoch. Photobio. A*, 1998, **116**, 209-214.
29. Y. Fu, J. Zhang, Y. Lv and W. Cao, *Spectrochim Acta A*, 2008, **70**, 646-650.
30. N. Sabbatini, M. Guardigli and J.-M. Lehn, *Coord. Chem. Rev.*, 1993, **123**, 201-228.
31. L. Winkless, R. H. C. Tan, Y. Zheng, M. Motevalli, P. B. Wyatt and W. P. Gillin, *Appl. Phys. Lett.*, 2006, **89**, 111115.
32. L. Armelao, S. Quici, F. Barigelletti, G. Accorsi, G. Bottaro, M. Cavazzini and E. Tondello, *Coord. Chem. Rev.*, 2010, **254**, 487-505.
33. O. Moudam, B. C. Rowan, M. Alamiry, P. Richardson, B. S. Richards, A. C. Jones and N. Robertson, *Chem. Commun.*, 2009, 6649-6651.
34. G. L. Law, T. A. Pham, J. D. Xu and K. N. Raymond, *Angew. Chem. Int. Edit.*, 2012, **51**, 2371-2374.
35. A. de Bettencourt-Dias, P. S. Barber and S. Bauer, *J. Am. Chem. Soc.*, 2012, **134**, 6987-6994.
36. J. D. Xu, T. M. Corneillie, E. G. Moore, G. L. Law, N. G. Butlin and K. N. Raymond, *J. Am. Chem. Soc.*, 2011, **133**, 19900-19910.
37. J. Yuasa, T. Ohno, K. Miyata, H. Tsumatori, Y. Hasegawa and T. Kawai, *J. Am. Chem. Soc.*, 2011, **133**, 9892-9902.
38. X. Q. Song, W. K. Dong, Y. J. Zhang and W. S. Liu, *Luminescence*, 2010, **25**, 328-335.
39. H. A. Azab, A. Duerkop, E. M. Saad, F. K. Awad, R. M. Abd El Aal and R. M. Kamel, *Spectrochim Acta A*, 2012, **97**, 915-922.
40. C. R. De Silva, J. Li, Z. P. Zheng and L. R. Corrales, *J. Phys. Chem. A*, 2008, **112**, 4527-4530.
41. A. Aebischer, F. Gumy and J. C. G. Bunzli, *PCCP*, 2009, **11**, 1346-1353.
42. X. O. Hu, W. Dou, C. Xu, X. L. Tang, J. R. Zheng and W. S. Liu, *Dalton Trans.*, 2011, **40**, 3412-3418.
43. Y. M. Zhu, M. Y. Xie, R. Zhang, Y. Y. Yang, C. H. Zeng, F. L. Zhao, Y. X. Tong, C. Y. Su and W. T. Wong, *Photoch Photobio Sci*, 2011, **10**, 1760-1765.
44. C.-H. Zeng, Y.-Y. Yang, Y.-M. Zhu, H.-M. Wang, T.-S. Chu and S. W. Ng, *Photochem. Photobiol.*, 2012, **88**, 860-866.
45. C. H. Zeng, F. L. Zhao, Y. Y. Yang, M. Y. Xie, X. M. Ding, D. J. Hou and S. W. Ng, *Dalton Trans.*, 2013, **42**, 2052-2061.
46. G. M. Sheldrick, University of Göttingen, University of Göttingen, Germany, 1997.
47. G. M. Sheldrick, in *version 5.1*, Bruker Analytical X-ray Instruments Inc., Madison, Wisconsin, 1998.
48. Z. Lin, R. Zou, W. Xia, L. Chen, X. Wang, F. Liao, Y. Wang, J. Lin and A. K. Burrell, *J. Mater. Chem.*, 2012, **22**, 21076-21084.
49. S. M. F. Vilela, D. Ananias, A. C. Gomes, A. A. Valente, L. D. Carlos, J. A. S. Cavaleiro, J. Rocha, J. P. C. Tome and F. A. Almeida Paz, *J. Mater. Chem.*, 2012, **22**, 18354-18371.
50. F. Terenziani, C. Le Droumaguet, C. Katan, O. Mongin and M. Blanchard-Desce, *Chemphyschem*, 2007, **8**, 723-734.
51. X. B. Zhang, J. K. Feng and A. M. Ren, *J Organomet Chem*, 2007, **692**, 3778-3787.
52. A. Picot, F. Malvolti, B. Le Guennic, P. L. Baldeck, J. A. G. Williams, C. Andraud and O. Maury, *Inorg. Chem.*, 2007, **46**, 2659-2665.
53. T. J. Sorensen, O. A. Blackburn, M. Tropiano and S. Faulkner, *Chem. Phys. Lett.*, 2012, **541**, 16-20.